ChemElectroChem

Articles
doi.org/10.1002/celc.202100978

Chemistry Europe
European Chemical
Societies Publishing

Special Collection

On the Savéant's Concerted/Stepwise Model. The Electroreduction of Halogenated Naphthalene Derivatives as a Case Study

Andrea Stefani,[a] Walter Giurlani,[b] Marco Bonechi,[b] Andrea Marchetti,[c] Giovanni Preda,[d] Dario Pasini,[d] Massimo Innocenti,[b, e, f, g] and Claudio Fontanesi*[h]

This paper is respectfully dedicated to Prof. Jean-Michel Savéant, in the view of his outstanding contribution in establishing and developing the "molecular electrochemistry" branch of science.

The electroreduction mechanism of 1-Br-2-naphtol and 1-I-2-naphtol, and of two inherently chiral BINOL derivatives ([1,1′-Binaphthalene]-2,2′-diol, 6,6′-dibromo and 1,1′-Binaphthalene,6,6′-dibromo-2,2′-dimethoxy; in the following named P1 and P2, respectively), is characterized by means of an integrated electrochemical and theoretical approach. The experimental characterization is based on cyclic voltammetry measurements. The experimental results indicate that the carbon halogen bond dissociates, following the electron uptake, with the formation of an insoluble final product (electro-polymerization). The reduction mechanism is assessed and disassembled at a molecular level by using DFT based quantum mechanical calculations. Both steady state, equilibrium, and kinetic (molecular dynamics, MD, DRC calculations) properties are calculated. A consistent picture is obtained by the comparison between experimental and theoretical results, indicating that the carbon-halogen bond dissociates following the first electron uptake, with a stepwise mechanism.

1. Introduction

In the field of organic reactivity, electrochemistry proves to be a powerful tool.[1,2] In particular, it can be used to study the dissociative dynamics of halogenated aromatic anions in condensed phase.[3–5] Electrochemical reduction of halogenated organic compounds has largely been studied for numerous crucial applications, just to mention a few: the degradation of environmental pollutants[6] and the synthesis of graphene-like films (by repeated covalent coupling of aryl radicals).[7] In fact, during these processes, the electron transfer (ET) is accompanied by the formation of radical species, which is possibly followed by the dissociation of the closed-shell halide anion. Figure 1 sets out the molecules studied in this paper.

The common base molecular framework consists of a 1-naphthol with a halogen substituent being Br or I in ortho position:1-Br-2-naphtol (**1**) and 1-I-2-naphtol (**2**). In the case of the Br substituent, two structurally related intrinsically chiral compounds have been synthesized and characterized electrochemically (in the view of possible further studies in the field of the so-called "spin-dependent electrochemistry"): **P1** and **P2**.[8,9] **P1** and **P2** feature two naphthalene-based units, which are connected, in the 1 position, by a single carbon-carbon bond.

In general, the electrochemical reduction of such class of compounds, leads to the bond dissociation of the carbon-halogen bond.[10,11] The electrochemical reduction of the neutral species leads to the formation of a negative radical anion, which is obtained by the injection of one electron. Note that,

[a] Dr. A. Stefani
Department of Physics, (FIM)
Univ. of Modena
Via Campi 213/A, 41125 Modena, Italy
[b] Dr. W. Giurlani, Dr. M. Bonechi, Prof. M. Innocenti
Department of Chemistry, "Ugo Schiff"
Univ. of Firenze
via della Lastruccia 3, 50019 Sesto Fiorentino, Italy
[c] Prof. A. Marchetti
Department of Chemical and Geological Science, DSCG
Univ. of Modena
Via Campi 103, 41125 Modena, Italy
[d] Dr. G. Preda, Prof. D. Pasini
Department of Chemistry
Univ. of Pavia
via Taramelli 10, 27100 Pavia, Italy
[e] Prof. M. Innocenti
National Interuniversity Consortium of Material
Science and Technology (INSTM)
Via G. Giusti 9, 50121 Firenze (FI), Italy
[f] Prof. M. Innocenti
Center for Colloid and Surface Science (CSGI)
Via della Lastruccia 3, 50019 Sesto F.no (FI), Italy
[g] Prof. M. Innocenti
Department of Industrial Engineering (DIEF)
University of Florence
Via di S. Marta, 3, 50139 Firenze, Italy
[h] Prof. C. Fontanesi
Department of Engineering "Enzo Ferrari", (DIEF)
Univ. of Modena
Via Vivarelli 10, 41125 Modena, Italy
E-mail: claudio.fontanesi@unimore.it

ChemElectroChem

Articles
doi.org/10.1002/celc.202100978

**Chemistry
Europe**
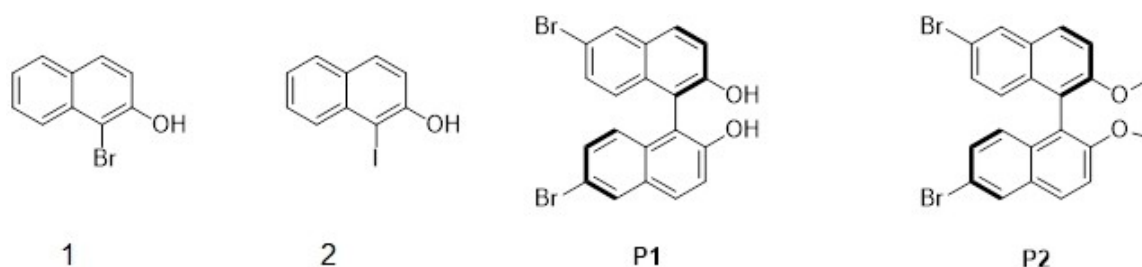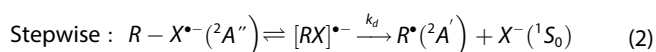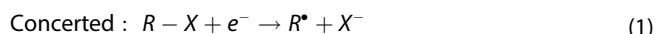European Chemical
Societies Publishing

Figure 1. Molecular structures of the compounds studied in this paper.

the carbon-halogen dissociation is observed also in studies concerning the collision between an electron beam and halogen-substituted organic compounds, in ultra-high vacuum.[12–16]

Indeed, a competition takes place between two different reaction schemes, as rationalized by Savéant: the carbon-halogen reaction path can follow a "concerted" or a "stepwise" mechanism.[10] As it is shown in equations (1) and (2), respectively.[11,17–20]

$$\text{Concerted}: \ R-X+e^{-} \rightarrow R^{\bullet}+X^{-} \tag{1}$$

$$\text{Stepwise}: \ R-X^{\bullet-}\left(^{2}A^{\prime\prime}\right) \rightleftharpoons [RX]^{\bullet-} \xrightarrow{k_{d}} R^{\bullet}\left(^{2}A^{\prime}\right)+X^{-}\left(^{1}S_{0}\right) \tag{2}$$

It is typically considered "stepwise" a mechanism where the intermediate radical anion species is actually formed, even in the case of an extremely short-lived species. The formation of the transient radical anion is due to the presence, in the pristine neutral parent compound, of a low-lying π type antibonding virtual MO, which is lower in energy than any σ type virtual MO. As a consequence, the π type radical anion features a lower energy than that of the σ radical anion (vide-infra). Compare Figure 2 for the relevant molecular orbital density distribution of the π and σ type radical anions. In the scenario of aromatic halides, which is the case presented in this study, the stepwise reaction is in general the preferred dissociation pathway. In particular, the π type radical anion is typically more stable than

the σ one for short carbon-halogen distances (characteristic of the neutral molecule). This picture is reversed as the carbon-halogen bond distance increases: the energy of the σ radical anion drops below that of the π type radical anion. On the contrary, in the "concerted" process the intermediate transient species has a lifetime which is shorter than the time of a bond vibration ($\approx 10^{-13}$ s).[21,22]

In this work, the electroreduction behaviour of 1, 2, P1 and P2 has been studied by cyclic voltammetry (CV) and chronoamperometry. The products of the electroreduction process are characterized by using HPLC-DAD chromatography, SEM imaging (and related EDX elemental analysis) for the deposit observed in the electroreduction of (1). Then, the carbon-halogen dissociation, of the radical anion species, has been theoretically studied by PES (Potential Energy Surface) analysis. In this way, a static picture of the system is obtained, and the energy of states featuring different electronic configurations can be compared. In particular, the radical anion produced by the first electron uptake is investigated, by a suitable (electronic molecular orbital "guess") selection of a π^* or σ^* molecular orbital configuration, where the spatial part of the unpaired highest in energy electron is described by a π^* or σ^* molecular orbital. The energy competition between the two different radical anion's configurations is explored as a function of the C–Br distance. Then, molecular dynamics (MD) calculations, within the Dynamical Reaction Co-ordinate (DRC) approach,[23] has been used to unfold the time-dependent evolution of the system.[24–27,22]
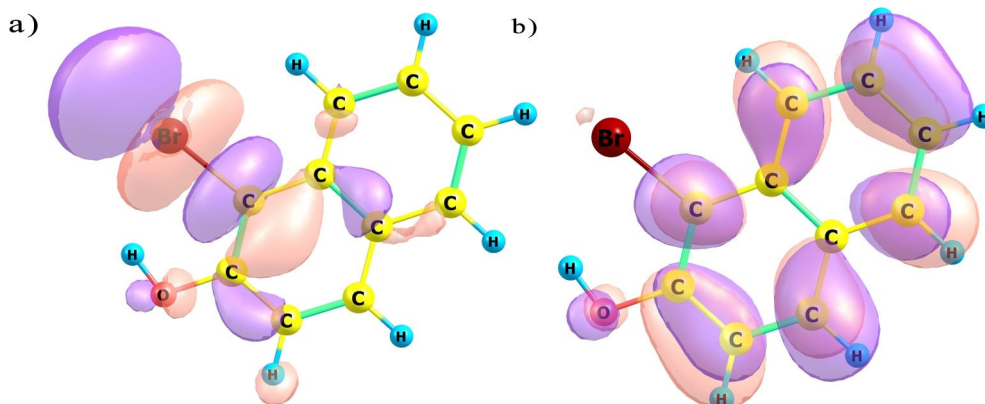

Figure 2. a) alpha SOMO of the σ radical, $\left(^{2}A^{\prime}\right)$ electronic state. b) alpha SOMO of the π radical, $\left(^{2}A^{\prime\prime}\right)$ electronic state.

ChemElectroChem

Articles
doi.org/10.1002/celc.202100978

Chemistry Europe
European Chemical
Societies Publishing

Experimental

Chemicals 1-Br-2-naphtol (**1**), 1-I-2-naphtol (**2**), tetrabutylammonium tetrafluoroborate (TBATFB) were purchased by Sigma. [1,1′-Binaphthalene]-2,2′-diol, 6,6′-dibromo (**P1**) and 1,1′-Binaphthalene, 6,6′-dibromo-2,2′-dimethoxy (**P2**) were synthesized as previously described.[28,29]

Cyclic voltammetry (CV) measurements were performed with an AUTOLAB PGSTAT type III using NOVA software from Metrohm Autolab. Rotating disk electrode (RDE) measurements were performed using a Metrohom Autolab RDE electrode. 1-Br-2-naphtol, 1-I-2-naphtol, P1 and P2 0,5 mmol dm^{-3} and TBA-TFB 0,1 mol dm^{-3} in acetonitrile solution were investigated between 0 and -1.3 V at different scan rate and different electrode rotation rate. Electrochemical measurements were performed using a three-electrode cell consisting of an Ag/AgCl/saturated KCl reference electrode (RE) a Pt counter electrode (CE) and a Pt working electrode (WE). The Pt working electrode was mechanically polished with 0.05 μm alumina, and subsequent electropolishing by scanning the potential at 100 mVs^{-1} between -0.2 and $+1.15$ V (vs. Ag/AgCl/KCl$_{sat}$) in 0,5 M H$_2$SO$_4$ solution until a reproducible curve was obtained. N$_2$ was used to purge the solution to achieve oxygen-free electrolyte solution.

Product characterization following the electroreduction

The products obtained by electroreduction of (1) were characterized by using High-Performance Liquid Chromatography equipped with a Diode Array Detector (HPLC-DAD). A Beckman System Gold chromatograph was used for HPLC-DAD chromatography. A reversed-phase column, Alltech C18 5 μm particle size, 150× 2.1 mm, was used for the separation of the reaction products, The separation was carried out using a linear gradient elution program with 0.1 % H$_3$PO$_4$ (A) and 100 % acetonitrile (B) for 30 minutes. The gradient elution program started with 30 % B for two min, 100 % B at 17 min for 8 min, 30 % B at 27 min until 30 for equilibration. The flow rate was 0.35 mL min^{-1} and the column temperature -25 °C. The injection volume was set to 20 μL. Diode-array detection was set to collect data in the range of 190 ÷ 500 nm.

Calculations were performed in the framework of ab initio quantum mechanical based methods with Gaussian[30] and Firefly[31] programs, using C1 symmetry and unrestricted wave function. Chemcraft[32] is used for visualization purposes, both molecular structures, and ab initio molecular orbitals display, and MacMolPlt[33]

served to display DRC trajectories. Original Fortran-based codes were created for the extraction of molecular geometrical parameters from DRC calculations, to allow for the analysis of angle and bond distance variations as a function of time (available on request from the author C.F.). Molecular geometries are obtained by full optimization carried out at B3LYP/6-311G(d) level of the theory.[34,35] Unrelaxed scan PES were performed to study both the dissociative path of halogenated radical anions and molecular orbital configuration in function of C—Br bond distance. To account for solute − solvent interaction, geometry optimization is carried out by using the Barone and Cossi's polarizable conductor model (CPCM).[36] In ab initio molecular dynamics, DRC trajectories (as implemented in the Firefly program) are started at molecular geometries of the radical anion. The velocity vector needed to start the molecular dynamics is obtained by the projection of Hessian vibrational eigenvectors. In the present DRC results the kinetic energy is partitioned over all normal modes, only the zero-point energy is assigned to each normal mode.

2. Results and Discussion

2.1. Electrochemical results

Figure 3a shows the cyclic voltammetry (CV) curve of 1-Br-2-naphtol. A reduction peak is evident in the forward scan between -1.0 and -1.1; the absence of the relevant oxidation peak in the backward scan implies that the reduction process is irreversible. The peak at -0.5 *V* is due to oxygen traces.

Figure 3b sets out linear voltammetry curves obtained at different WE angular rotation speed, ω (by using a rotating disk electrode, RDE). A linear relation is obtained between the "limiting" current values at -1.1 V and $\omega^{1/2}$, compare Figure 3b inset. The Levich equation is used to fit the data shown in Figure 3b,[37] aiming to determine the diffusion coefficient and molecular radius (by means of the Stokes-Einstein equation): $I_L = 4.2 \times 10^{-5}\ \omega^{1/2}$ is obtained by the least square fit of the data in Figure 3b inset. From the slope of Levich equation, the diffusion coefficient D results as $4.5 \times 10^{-7}\ cm^2 s^{-1}$; assuming *i)* the number of exchanged electrons, *n*, equal to 1 *ii)* the
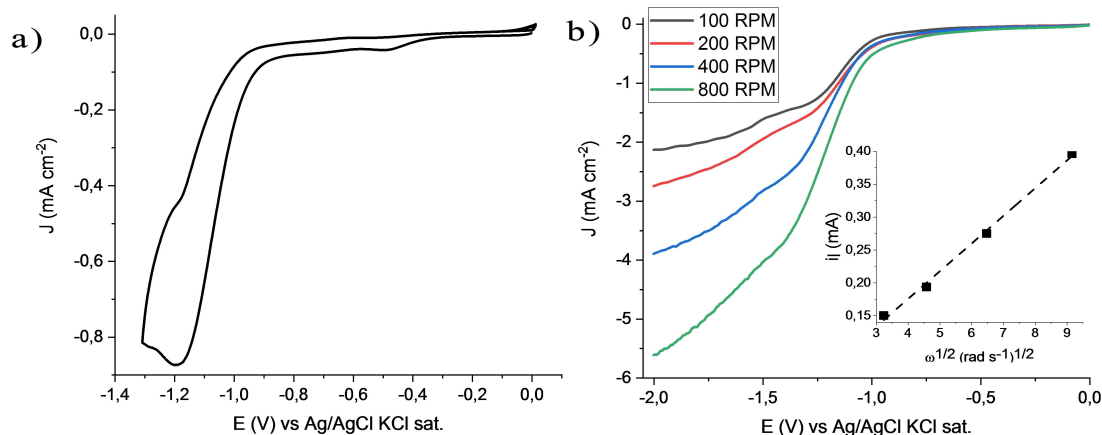

Figure 3. Voltammetry curves of a 1-Br-2-naphtol 5 mM, in 0.1 M TBATFB acetonitrile solution, 3 mm radius Pt disk electrode WE. Scan rate 50 *mVs*$^{-1}$ a) CV curve, first cycle, b) Cyclic voltammetry curves as a function of the angular rotation speed. The inset shows the graph of the limiting current, I_L, vs the square root of the angular rotation speed: $I_L = 4.2 \times 10^{-5}\ \omega^{1/2}$.

ChemElectroChem

Articles
doi.org/10.1002/celc.202100978

Chemistry
Europe
European Chemical
Societies Publishing

kinematic viscosity of the solution is considered $4.9 \times 10^{-3}\ cm^2 s^{-1}$ (i.e. the value corresponding to the pure acetonitrile). Then by using the Stokes-Einstein relation a molecular radius of about 9.9 Å is obtained, which is a result consistent with the size of 1-Br-2-naphtol (about 5.2 Å, van der Waals radii) solvated by a single solvation shell. Eventually, it must be noted that upon electroreduction the 1-Br-2-naphtol yields a dark-brown insoluble deposit on the WE surface (see figure S5 in the Supporting Information). This is consistent with the carbon bromine dissociation, featuring a subsequent follow-up reaction involving the naphthyl aryl neutral radicals. In the cyclic voltammetry shown in figures S1, it can be noted that the reduction of the 1-I-2-naphthol reagent occurs at more

negative potentials, with respect to the 1-Br-2-naphthol. Table 1 reports the potential and peak current experimental values.

Figure 4 sets out the HPLC-DAD chromatograms before and after electroreduction of the solution of 1-Br-2-naphtol, Figure 4a and Figure 4b respectively. Figure 4c shows the UV-Vis spectrum of the pristine solution, corresponding to the spectrum relevant to the chromatogram peak at $t=14.3$ in Figure 4a (pristine solution). Figure 4d shows the UV-Vis spectrum of the solution after electroreduction, corresponding to the spectrum relevant to the chromatogram peak at $t=18.4$ in Figure 4b (a 3D representation, mAU vs wavelength vs time, of the 2D results shown in Figure 4, can be found in the Supporting Information section 2.3: Figure S9). Spectra in Figures 4c and 4d are qualitatively similar, save a prominent difference in the ratio between the absorption peaks. Indeed, the ratio in absorption between the 280 and 230 nm peaks varies from 0.08 (pristine solution) to 0.13 (after electrochemistry). This result is consistent with the theoretical UV-Vis spectra, compare section 2.4 of the Supporting Information (figure S10), and it is in agreement with the decrease of the concentration of 1-Br-2-naphtol in solution accompanied by the formation of a dimer.

Moreover, the morphology of the film formed on the electrode by the electroreduction of 1, was characterized by optical and electronic microscopy (SI, section 2.1, 2.2, figures S6,

Table 1. Experimental and theoretical results. Columns 2 and 3, report the values of peak potential (E_p) and peak current density (I_p). Column 4 reports the energies of the lowest unoccupied molecular orbital (LUMO), neutral species, B3LYP/6-311G(d)//HF/6-311G(d).

Compound	$E_p[V]$[a,b]	$I_p[mA\ cm^{-2}]$[a,b]	LUMO Energy [eV]
1-Br-2-naphthol	−1.20	−0.85	2.0735
1-I-2-naphthol	−1.50	−0.95	2.0495
P1	−1.55	−1.35	1.9913
P2	−2.00	−2.10	2.0329

[a] potential values vs Ag/AgCl/KCl$_{sat}$; [b] scan rate 50 mVs^{-1}.
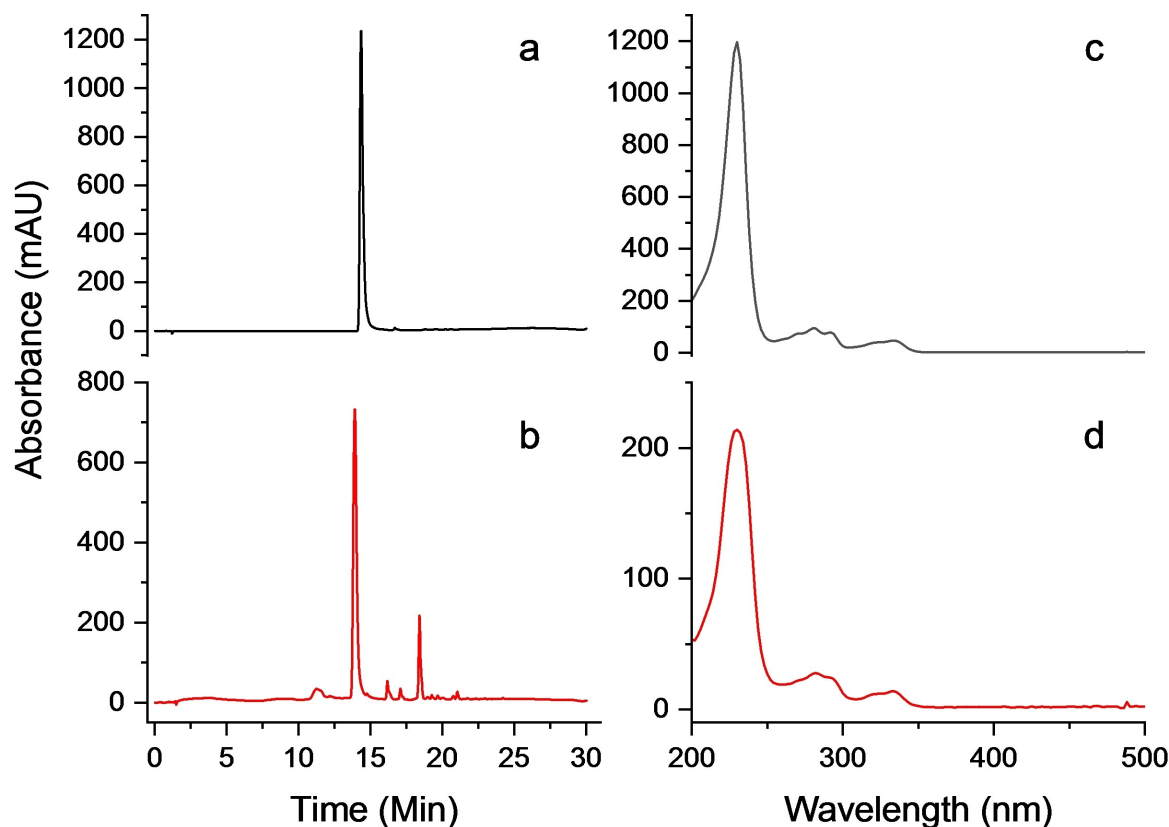

Figure 4. HPLC-DAD chromatograms of the solution of (1) in ACN: a) pristine solution, before electrochemistry b) after 15 minutes chronoamperometry at −1.1 V constant potential for 15 minutes. UV-Vis DAD spectra: c) relevant to the pristine solution (i.e. the spectrum corresponding to the peak present at $t=14.3$ minutes in chromatogram a) d) spectrum relevant to the solution after electroreduction (in this case the spectrum corresponds to the peak present at $t=18.4$ minutes in chromatogram b).

ChemElectroChem

Articles
doi.org/10.1002/celc.202100978

Chemistry
Europe
European Chemical
Societies Publishing

S7). EDS analysis proves that the film does not contain bromine (compare Section 2.2 of the supporting Information, figure S.8). What is more, the addition of AgNO₃ to the electrolysis solution of 1, after electroreduction, yields the formation of a precipitate. The X-ray fluorescence analysis shows that the precipitate is AgBr (SI, section 2.6, figure S12). Thus, all the multitude of the experimental results gives sound basis to the idea that upon the electron uptake, 1 forms a radical anion which dissociates following reaction (2).

2.2. Theoretical results

The calculation of the standard reduction potential $E°$ was carried out by using the Nernst equation $\Delta G^0 = -nFE^0$. The standard Gibbs energy $\Delta G°$ is determined vs. the NHE reaction,[38–40] as a sum of the two contributions due to the $RX/[RX]^{•-}$ couple and hydrogen reduction half reaction $\Delta G^0_{H^+/H_2}$, compare equation (3). A value of 4.44 eV has been assigned to $\Delta G^0_{H_2/H^+}$.[41] The $\Delta G^0_{RX/[RX]^{•-}}$ value has been calculated by the difference in total electronic energy calculated between the neutral and radical anion species, at the B3LYP/6-311G(d) level of theory. The Barone and Cossi polarizable conductor model (CPCM) method has been used to account for solute-solvent interaction.[42,36]

$$-nFE^0_{RX/[RX]^{•-} \; vs \; NHE} =$$
$$\Delta G^0_{RX/[RX]^{•-} \; vs \; NHE} = \Delta G^0_{RX/[RX]^{•-}} + \Delta G^0_{H^+/H_2} \qquad (3)$$

Table 1 reports both experimental as well as theoretical standard potential for close comparison.

Figure 5 sets out the potential energy curves, and MOs correlation diagram, for the 1-Br-2-naphthol radical anion, doublet $^2A'$ (σ radical) and $^2A''$ (π radical) electronic states (vide supra Figure 2 for the graphical representation of the relevant MOs), as a function of the carbon-bromine bond distance, d_{C-Br}.

The $^2A''$ (π radical, blue circles) potential energy curve vs. C − Br bond distance features a "Morse-like" pattern of associative nature. A minimum is present for $d_{C-Br} = 1.9466$ Å (optimized geometry at the B3LYP/6-311G(d) level of the theory, Cs symmetry). Please note that for the $^2A''$ electronic state the dissociation is predicted to be a global up-hill in energy process, i.e. it is a bound state. On the contrary, the PES relevant to the $^2A'$ (σ radical) electronic state (red circles Figure 5a) shows a monotonous decreasing pattern as a function of d_{C-Br}; with energy values larger than the π radical ones for d_{C-Br} values typical of the neutral, $^1S_0$, ground state. While for $d_{C-Br} \cong 2.2$ Å the $^2A'$ (σ radical) and $^2A''$ (π radical) electronic states energies are degenerate in energy. Then, as the carbon bromine bond distance increases, the $^2A'$ energy is lower than the $^2A''$ one. As a whole in the range of short d_{C-Br} distances the π radical is more stable than the σ one. The opposite holds for carbon bromine distances larger than 2.2 Å Indeed, the SOMO transformation from $^2A''$ to $^2A'$ orthogonal wavefunctions is forbidden by symmetry. Figure 5b sets out the relevant correlation diagram concerning the "transformation" of MOs involved in reaction (2) going from initial state (radical anion) to the products aryl radical and halogen anion (in this case bromide or iodide). The electron couple involved in the carbon halogen bond transforms in a lone-pair couple localized on the halogen anion, without any change of symmetry. The unpaired electron spatial part transforms from A'' to A', which is symmetry forbidden: allowed crossing.[16] The dissociative reaction can proceed via a symmetry lowering of the radical anion, the latter occurs via some suitable distortion of the molecular geometry,[16,17] which destroys the original orthogonality of the $^2A'$ and $^2A''$ states. Thus, the radical formed upon the first electron uptake (reduction) will feature some stability. Then, the destruction of symmetry due vibrational modes able to mix the two orthogonal $^2A'$ and $^2A''$ electronic states, allows for the takeover of the $^2A'$ potential energy surface. Eventually making possible the carbon bromine bond dissociation. A point open to discussion is the dynamics of the overall dissociation
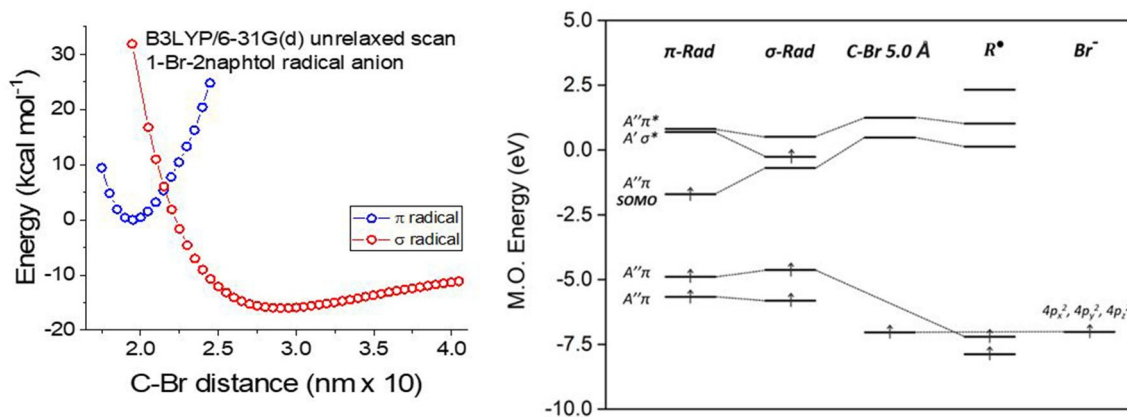

Figure 5. 1-Br-2-naphthol radical anion, B3LYP/6-311G(d) level of the theory. a) $^2A'$ (σ radical, red circles) and $^2A''$ (π radical, blue circles) electronic states potential energy curves vs. C − Br bond distance b) MOs correlation diagram for the α orbitals. On the left, the graph shows MOs ordering following the electron uptake, depending on the π or σ nature of the MO which describes the spatial part of the unpaired electron. The electronic configurations associated to a long 5.0 Å carbon bromine (bromide) distance is also presented. After the dissociation, the correlation between the A'' MO of the radical R• and the three 4p lone pairs of the bromide anion is outlined on the right.

ChemElectroChem

Articles
doi.org/10.1002/celc.202100978

**Chemistry
Europe**
European Chemical
Societies Publishing

process. This is a subject virtually impossible to study experimentally due to a number of complicating factors: it is a very fast process in a condensed phase with the presence of a number of other compounds (base electrolyte and solvent), the concentration of the radical anion is extremely low. In this case a theoretical approach is the only viable approach: molecular dynamics (MD). The dynamics of the electroreduction process is characterized by using the dynamic reaction coordinate (DRC) method.[23] Which is a classical dynamic calculation based on an ab-initio potential energy surface. Figure 6 shows the results of a typical DRC calculations, B3LYP/6-311G(d) level of the theory, carried out in the case of the 1-Br-2-naphtol radical anion. In screening calculations DRC trajectories are calculated starting from the Cs full optimized geometry of the neutral parent 1-Br-2-naphtol neutral species. In DRC calculations the most important decision concerns a suitable selection of the initial velocity vector (in the case of a molecule made by n centers, atoms, a DRC input necessitates of $6n$ initial values, i.e. $3n$ geometrical coordinates and $3n$ velocity vectors). The DRC trajectory whose results are reported in Figure 6, is obtained by

partitioning the, initial, system kinetic energy over each normal mode. Then, the initial velocity vector is obtained by projecting the Hessian matrix obtained by a previous calculation run on the parent neutral 1-Br-2-naphtol, closed shell, species. Initial kinetic energy is obtained assigning only the zero-point energy to each normal mode. A number of interesting information can be obtained by the analysis of the DRC trajectory: potential energy, carbon dissociating-bond distance (d_{C-Br}), dihedral angle variation) as a function of time. The energy as a function of time, Figure 6a, is characterized by a quite evident ripple, the ripple is due to the vibrational modes. Figure 6b displays the variation of d_{C-Br} as a function of time, remarkably there is a sudden, almost vertical increase in the 150 to 200 fs time interval. This correspond to a sort of discontinuity in the energy vs t curve, which is followed by a decrease in the average energy of about 15 kcal mol^{-1}. Figure 6b shows a sort of a maximum in the dihedral angle formed by the bromine atom with the aromatic plane. Thus, after an initial "incubation" time of about 150 fs, the dissociation occurs in about 50 fs. This is marked by a sudden minimum in the potential energy at 180 fs,
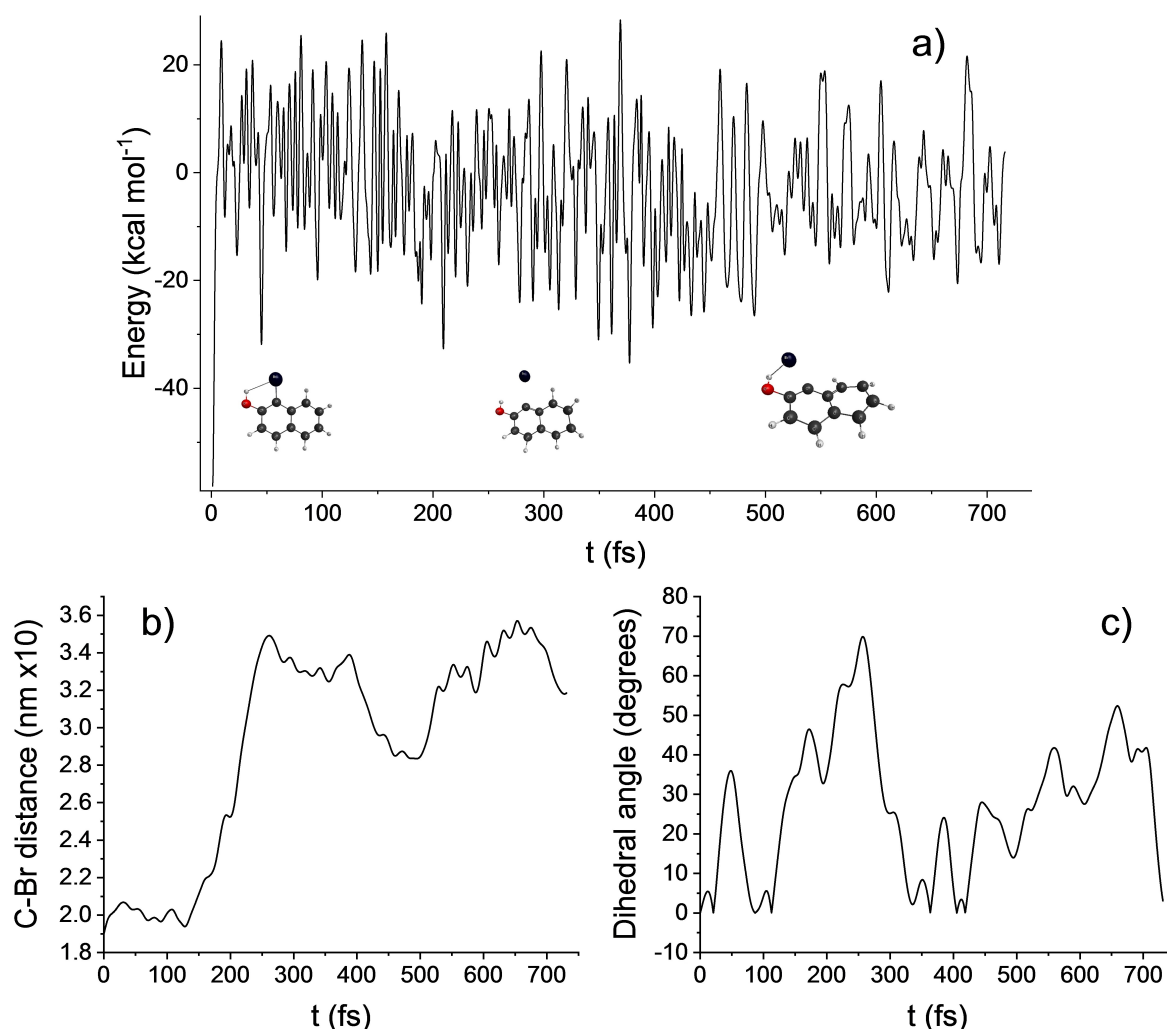

Figure 6. a) 1-Br-2-naphtol DRC trajectory for the doublet radical anion. The graph shows the molecular electronic energy as a function of the time. b) Carbon bromine (bromide, since the charge on Br is minus one for time values larger than 200 fs) distance as a function of time c) dihedral angle between the dissociating $C-Br$ bond as a function of the time.

ChemElectroChem

Articles
doi.org/10.1002/celc.202100978

Chemistry Europe
European Chemical
Societies Publishing

Figure 6a, being a constant total energy dynamics, this implies a sudden maximum in the kinetic energy (the related to an increase in the velocity of the dissociating bromide anion). Thus, both the PES analysis based on Figure 3 steady state results, as well as the MD data obtained from the DRC calculations give due reason to the formation of an initial transient π type radical anion, which evolves in an extremely short time. In fact, DRC calculations were carried out in the presence of a theoretical dielectric-continuum solvent. Thus, electronic based solvent effect is present, but not any viscosity (mechanically) related contribution (which could lead to an increase in the dissociation time).

3. Conclusion

The dynamics of the dissociative electroreduction of naphthalene halogen derivatives is characterized by means of an integrated electrochemical and theoretical approach. This allows to propose a consistent mechanism for the electro-reductive dissociation of the carbon halogen (Br or I), which is investigated in detail at a molecular level by close comparison with theoretical results: analysis of the electron configuration molecular energies of the π and σ radicals as a function of the dissociating bond length, PES vs. $C-Br$ bond distance. Eventually, DRC calculations allow to shed light on the geo-metrical variation as a function of time of the radical anion as a function of the progress of the dissociative process. In summary, on the effect of molecular structure on the fate of the radical anion upon the electroreduction:

1 it leads to the formation of an insoluble film on the surface of the working electrode. This gives strong indication of a follow-up reaction involving the radicals formed upon the carbon-halogen dissociation.

2 What is more, **P1** and **P2** seem to give rise to a more stable radical anion, without dimer cross-coupling between the radicals (a result which can be exploited to induce chirality upon reaction with the radical anion).

This approach is meant to provide precious information needed to design and select suitable molecular architectures tailored for the cross-coupling between radicals obtained under electroreductive regime with radicals yielded via electrochem-ical oxidation. These peculiar experimental findings are the subject of current investigation in our lab.

Acknowledgements

Conflict of Interest

The authors declare no conflict of interest.

[1] J.-M. Savéant, in *Advances in Physical Organic Chemistry*, Elsevier, **1990**, pp. 1–130.
[2] V. V. Zhuikov, *Russ. J. Electrochem.* **2000**, *36*, 117–127.
[3] C. Fontanesi, *J. Mol. Struct. THEOCHEM* **1997**, *392*, 87–94.
[4] C. Lei, F. Liang, J. Li, W. Chen, B. Huang, *Chem. Eng. J.* **2019**, *358*, 1054–1064.
[5] A. Cardinale, A. A. Isse, A. Gennaro, M. Robert, J.-M. Savéant, *J. Am. Chem. Soc.* **2002**, *124*, 13533–13539.
[6] E. T. Martin, C. M. McGuire, M. S. Mubarak, D. G. Peters, *Chem. Rev.* **2016**, *116*, 15198–15234.
[7] Z. Kudaş, E. Gür, D. Ekinci, *Langmuir* **2018**, *34*, 7958–7970.
[8] T. S. Metzger, S. Mishra, B. P. Bloom, N. Goren, A. Neubauer, G. Shmul, J. Wei, S. Yochelis, F. Tassinari, C. Fontanesi, D. H. Waldeck, Y. Paltiel, R. Naaman, *Angew. Chem. Int. Ed.* **2020**, *59*, 1653–1658.
[9] F. Tassinari, J. Steidel, S. Paltiel, C. Fontanesi, M. Lahav, Y. Paltiel, R. Naaman, *Chem. Sci.* **2019**, *10*, 5246..
[10] C. P. Andrieux, J.-M. Savéant, A. Tallec, R. Tardivel, C. Tardy, *J. Am. Chem. Soc.* **1997**, *119*, 2420–2429.
[11] C. P. Andrieux, J. M. Saveant, D. Zann, *Nouv. J. Chim.* **1984**, *8*, 107–116.
[12] J. C. Steelhammer, W. E. Wentworth, *J. Chem. Phys.* **1969**, *51*, 1802–1814.
[13] G. Distefano, A. Modelli, M. Guerra, D. Jones, S. Rossini, *J. Mol. Struct.* **1988**, *174*, 177–182.
[14] T. M. Stephen, X. Shi, P. D. Burrow, *J. Phys. B* **1988**, *21*, L169–L171.
[15] J. M. Dreiling, T. J. Gay, *J. Phys. Conf. Ser.* **2015**, *635*, 012015–012024.
[16] J. M. Dreiling, F. W. Lewis, T. J. Gay, *J. Phys. B* **2018**, *51*, 21LT01.
[17] J.-M. Savéant, in: *Advances in Physical Organic Chemistry* (Ed.: D. Bethell), Academic Press, **1990**, pp. 1–130.
[18] C. Costentin, M. Robert, J.-M. Savéant, *Acc. Chem. Res.* **2010**, *43*, 1019–1029.
[19] C. Amatore, *Basic Concepts in "Organic Electrochemistry: Revised and Expanded" Edited by Ole Hammerich and Bernd Speiser*, CRC Press Taylor & Francis Group, Boca Raton, **2015**.
[20] E. Deunf, E. Labbé, J. N. Verpeaux, O. Buriez, C. Amatore, *RSC Adv.* **2012**, *2*, 5398–5402.
[21] S. Eldin, W. P. Jencks, *J. Am. Chem. Soc.* **1995**, *117*, 4851–4857.
[22] C. Fontanesi, P. Baraldi, M. Marcaccio, *J. Mol. Struct. THEOCHEM* **2001**, *548*, 13–20.
[23] J. J. P. Stewart, L. P. Davis, L. W. Burggraf, *J. Comput. Chem.* **1987**, *8*, 1117—1123.
[24] L. Benedetti, G. B. Gavioli, C. Fontanesi, *J. Chem. Soc. Faraday Trans.* **1990**, *86*, 329–334.
[25] G. B. Gavioli, M. Borsari, C. Fontanesi, *J. Chem. Soc. Faraday Trans.* **1993**, *89*, 3931–3939.
[26] R. Andreoli, G. B. Gavioli, M. Borsari, C. Fontanesi, *J. Chem. Soc. Faraday Trans.* **1994**, *90*, 3241–3244.
[27] T. Taketsugu, M. S. Gordon, *J. Phys. Chem.* **1995**, *99*, 8462–8471.
[28] M. Agnes, A. Nitti, D. A. V. Griend, D. Dondi, D. Merli, D. Pasini, *Chem. Commun.* **2016**, *52*, 11492–11495.
[29] M. Agnes, A. Arabi, M. Caricato, A. Nitti, D. Dondi, K. Yannakopoulou, M. Patrini, D. Pasini, *ChemPlusChem* **2021**, *86*, 270–274.
[30] J. A. Pople, *Gaussian Suite of Programs*, Wallingford, Connecticut, **2017**.
[31] A. Granovsky A, *Firefly Version 8.0.0*, http://Classic.Chem.Msu.Su/Gran/Firefly/Index.Html, **2016**.
[32] G. A. Andrienko, *Chemcraft - graphical software for visualization of quantum chemistry computations.*, "Chemcraft - graphical software for visualization of quantum chemistry computations.," can be found under https://www.chemcraftprog.com, **2021**.
[33] B. M. Bode, M. S. Gordon, *J. Mol. Graphics Modell.* **1998**, *16*, 133–138.
[34] M. Marcaccio, F. Paolucci, C. Fontanesi, G. Fioravanti, S. Zanarini, *Inorg. Chim. Acta* **2007**, *360*, 1154–1162.
[35] C. Bruno, F. Paolucci, M. Marcaccio, R. Benassi, C. Fontanesi, A. Mucci, F. Parenti, L. Preti, L. Schenetti, D. Vanossi, *J. Phys. Chem. B* **2010**, *114*, 8585-8592.

[36] M. Cossi, N. Rega, G. Scalmani, V. Barone, *J. Comput. Chem.* **2003**, *24*, 669–681.

[37] A. J. Bard, L. R. Faulkner, *Wiley: Electrochemical Methods: Fundamentals and Applications, 2nd Edition*, Wiley, New York, **2001**.

[38] S. Trasatti, *J. Electroanal. Chem. Interfacial Electrochem.* **1983**, *150*, 1–15.

[39] P. Winget, E. J. Weber, C. J. Cramer, D. G. Truhlar, *Phys. Chem. Chem. Phys.* **2000**, *2*, 1231–1239.

[40] P. Winget, C. J. Cramer, D. G. Truhlar, *Theor. Chem. Acc.* **2004**, *112*, 217–221.

[41] S. Trasatti, *Electrochim. Acta* **1990**, *35*, 269–271.

[42] V. Barone, M. Cossi, *J. Phys. Chem. A* **1998**, *102*, 1995–2001.